RGMa modulates T cell responses and is involved in autoimmune encephalomyelitis

Rieko Muramatsu, Takekazu Kubo, Masahiro Mori, Yuka Nakamura, Yuki Fujita, Tsugio Akutsu, Tatsusada Okuno, Junko Taniguchi, Atsushi Kumanogoh, Mari Yoshida, Hideki Mochizuki, Satoshi Kuwabara and Toshihide Yamashita

Supplementary Information

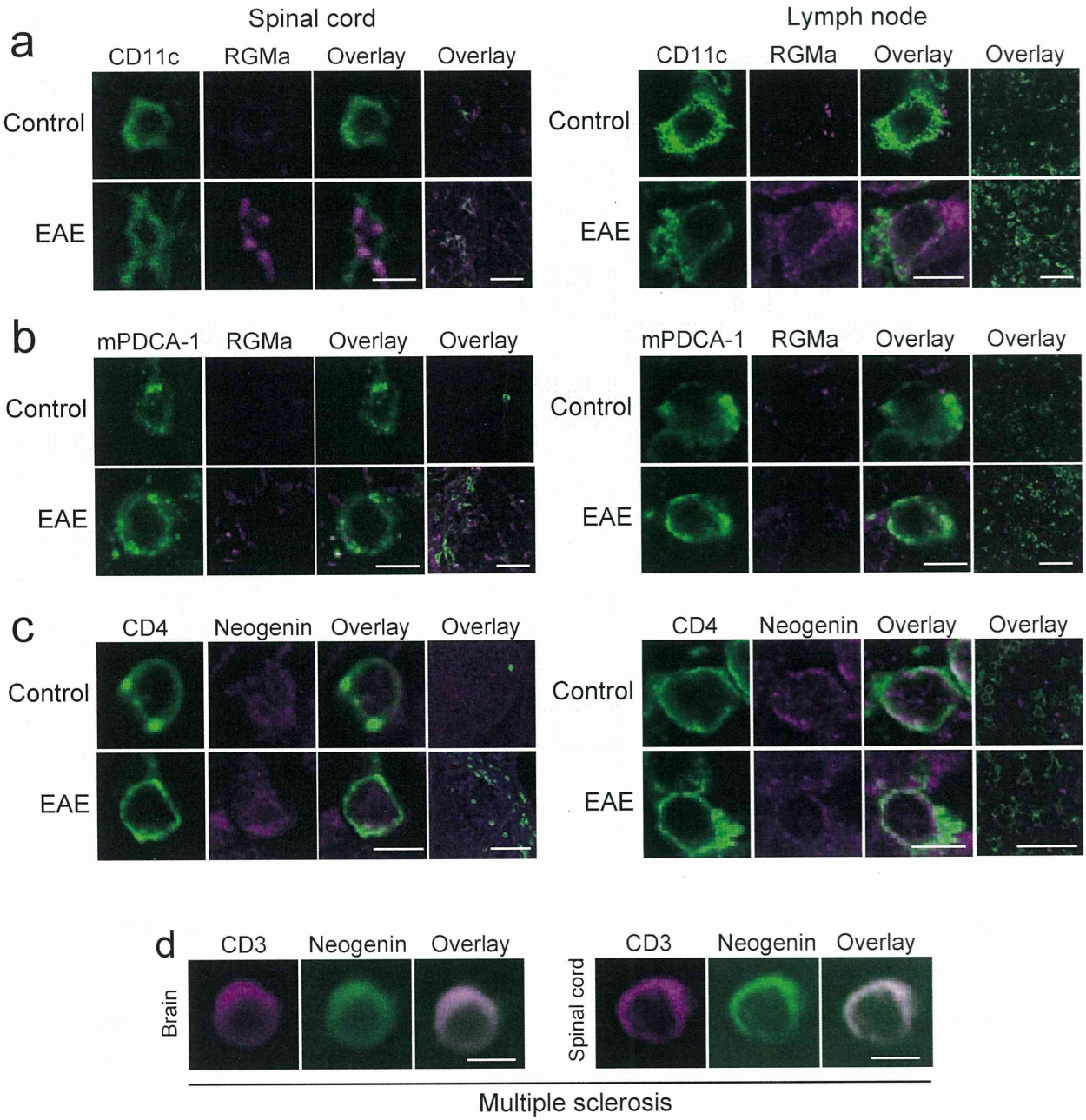

Supplementary Figure 1. Immunostaining for RGMa and neogenin in sections from MOG-EAE mice and individuals with MS. (a–c) Immunostaining for RGMa and neogenin expressions in combination with CD11c (a), mPDCA-1 (b), and CD4 (c) in lymph node and spinal cord sections from MOG-EAE and control mice. For details, please refer to Fig. 2a–c. Scale bar, 10 μm for high and 50 μm for low magnification images. **(d)** Double-labeling of brain and spinal cord sections with MS for neogenin and CD3. *n* = 8, scale bar = 5 μm.

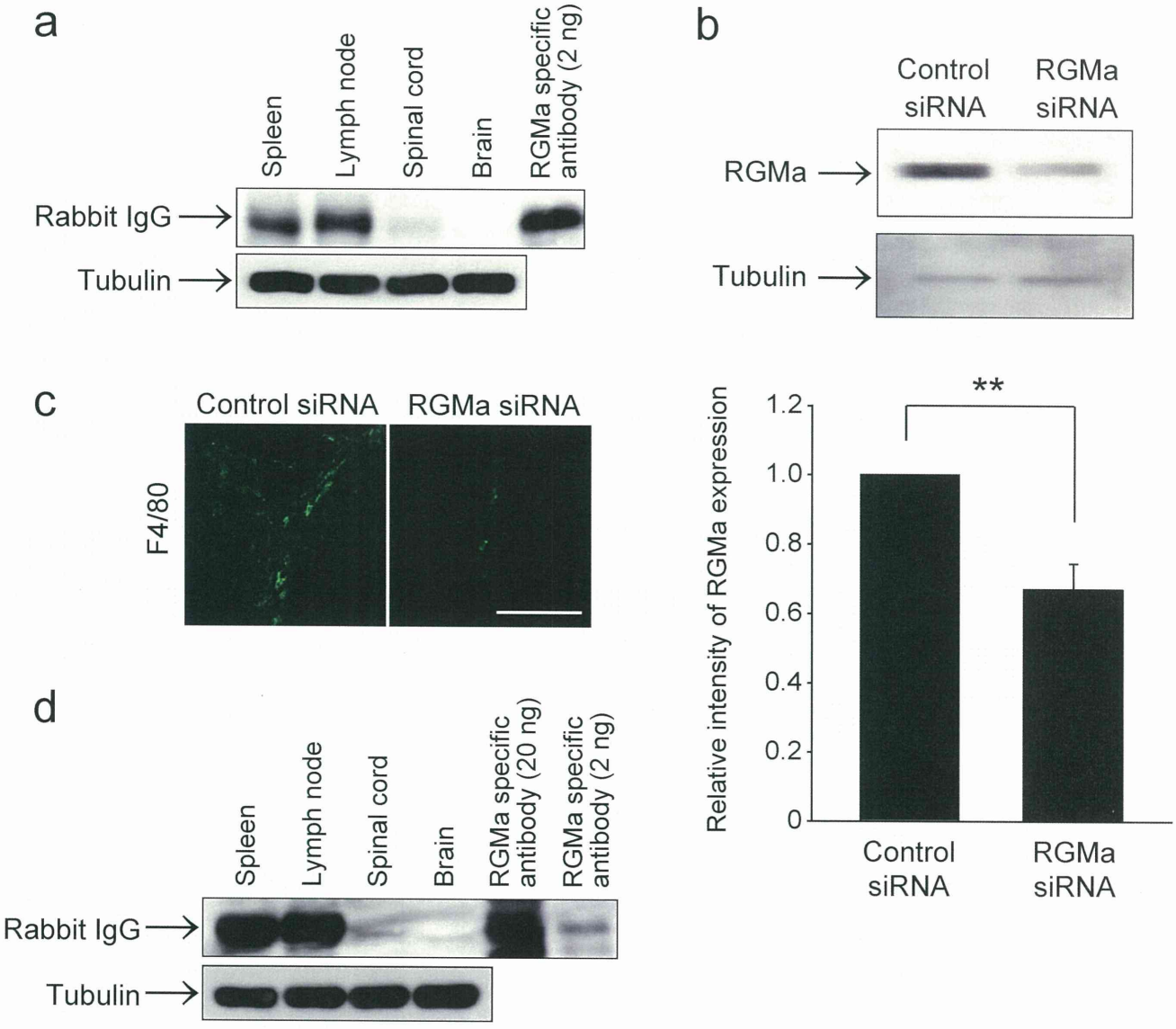

Supplementary Figure 2. Distribution of RGMa-specific antibody in mice and knockdown of RGMa expressions. (a) Western blots for detecting RGMa-specific antibody in several organs on d 7 after administration. **(b)** Western blots for detecting RGMa expression in RGMa siRNA-transfected BMDCs. The graph shows the relative expressions of RGMa. $^{**}P < 0.01$ by Student's *t*-test. **(c)** Representative images showing the presence of F4/80-positive cells in the spinal cord after the adoptive transfer of antigen-stimulated BMDCs with or without RGMa knockdown. The spinal sections were obtained at d 21 after EAE induction. Scale bar = 200 μm. **(d)** Western blots for detecting RGMa-specific antibody in several organs on d 11 after MOG immunization. RGMa-specific antibodies were administered by intraperitoneal injection to mice at d 7 and 10 after MOG immunization.

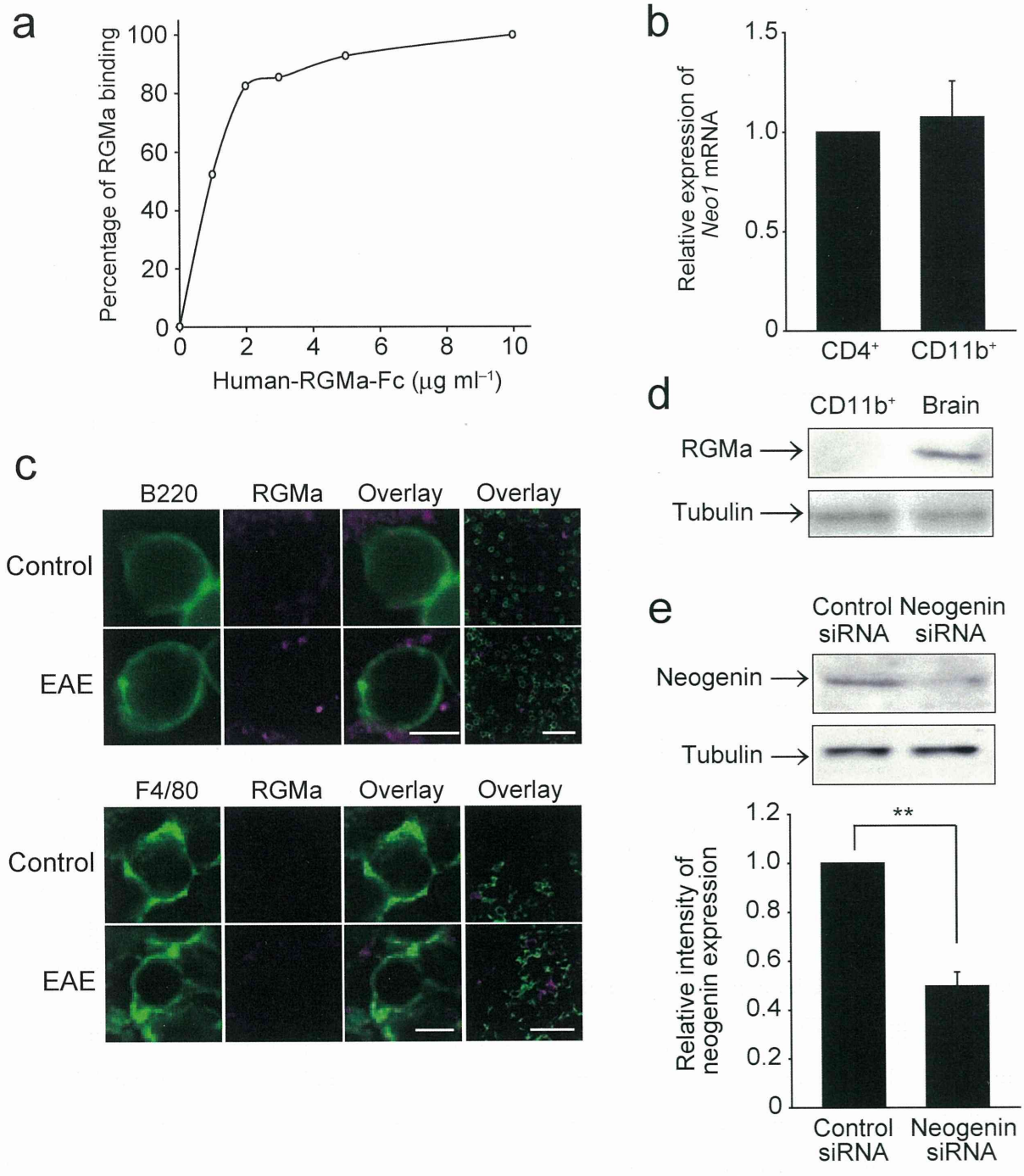

Supplementary Figure 3. Determination of RGMa and neogenin expressions. (a) Binding of human RGMa-Fc (indicated concentrations) to CD11b$^+$ cells in the spleen. **(b)** Relative expression of *Neo1* mRNA by RT-PCR analysis in CD4$^+$ T cells and CD11b$^+$ cells from the mouse spleen. The values represent the mean ± SEM of three independent experiments. **(c)** Immunostaining for RGMa in B220$^+$ cells or F4/80-positive macrophages from the spleen of MOG-EAE mice. Scale bar, 10 μm for high and 50 μm for low magnification images. **(d)** Western blots for RGMa expression in CD11b$^+$ macrophages isolated from the spleen of MOG-EAE mice and in the brain. **(e)** Western blots for detecting neogenin expression in neogenin siRNA-transfected BMMØs. The graph shows the relative expressions of neogenin. $^{**}P < 0.01$ by Student's *t*-test.

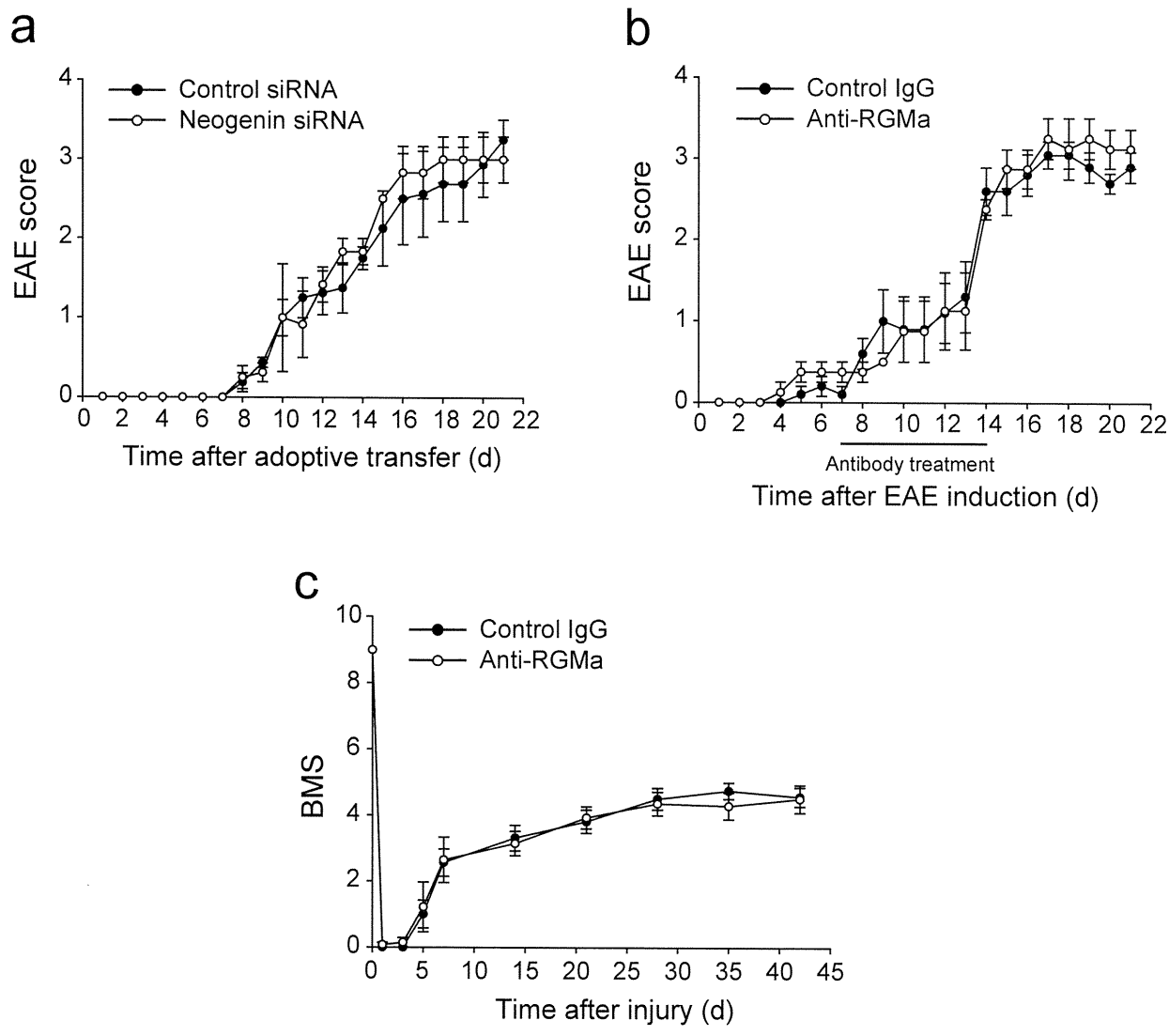

Supplementary Figure 4. Assessment of the *in vivo* mechanism of action of RGMa-specific antibody. (a) EAE scores in the CD11b-DTR mice that received adoptive transfer of macrophages with neogenin siRNA or control siRNA transfection (control siRNA, $n = 5$; neogenin siRNA, $n = 5$). **(b)** The progression of MOG-induced EAE in C57BL/6 mice after intrathecal administration of RGMa-specific antibody or control IgG in the cervical spinal cord (control IgG, $n = 4$; RGMa-specific antibody, $n = 5$). **(c)** BMS scores determined at the indicated time points after spinal cord contusion injury in mice intraperitoneally injected with control IgG or RGMa-specific antibody (control IgG, $n = 8$; RGMa-specific antibody, $n = 7$). All values represent the mean ± SEM (Mann–Whitney's *U* test).

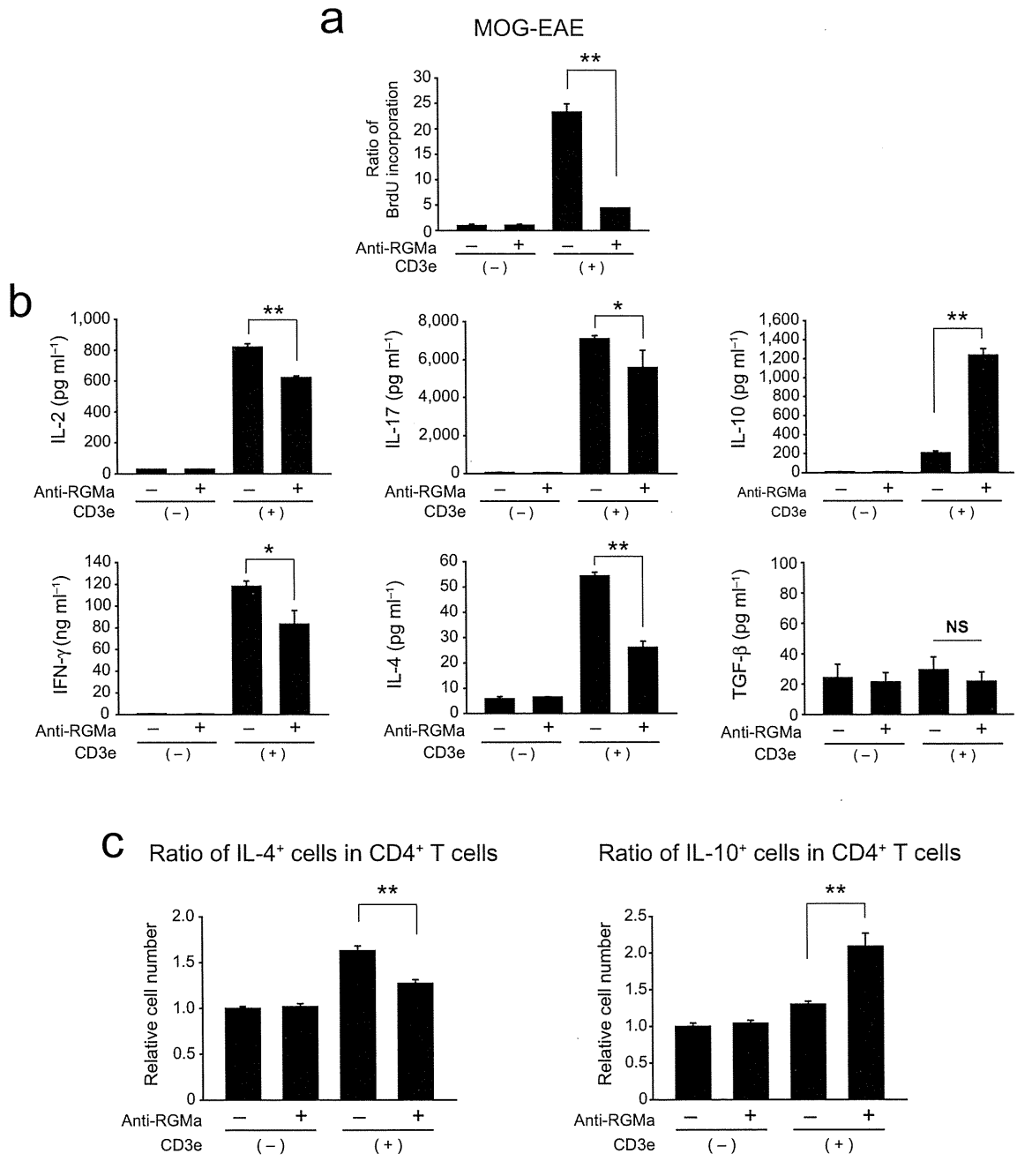

Supplementary Figure 5. T-cell responses to CD3-specific antibody in mice treated with RGMa-specific antibody or control IgG. (a) CD3-specific antibody-elicited proliferative responses in splenocytes obtained from mice treated with RGMa-specific antibody or control IgG on d 21 after the MOG immunization (control IgG, *n* = 6; RGMa-specific antibody, *n* = 5). **(b)** Production of IL-2, IL-4, IL-10, IFN-γ, TGF-β, and IL-17 by splenocytes obtained from mice treated with RGMa-specific antibody or control IgG (control IgG, *n* = 6; RGMa-specific antibody, *n* = 5). **(c)** The relative number of IL-4-producing T cells and IL-10-producing T cells with or without the RGMa-specific antibody treatment (*n* = 3 for each group). All values represent the mean ± SEM. **P* < 0.05, ***P* < 0.01 by Student's *t*-test.

SUPPLEMENTARY METHODS

Cell preparation. We pressed freshly isolated spleens of C57BL/6 mice gently in RPMI-1640 medium (Invitrogen) and treated them with ACK lysing buffer (Lonza Walkersville) to remove erythrocytes. After washing thrice with RPMI-1640 medium, we filtered the cell suspension through a 70 μm cell strainer to obtain a single-cell suspension of splenocytes. We purified the $CD4^+$ T cells, $CD11b^+$ macrophages, and $CD45R^+$ B cells from the splenocytes by positive sorting, using CD4-, CD11b-, and CD45R-specific antibody-coated magnetic beads, respectively (Miltenyi Biotec). Further, we prepared BMDCs and BMMØs by culturing bone marrow cells with granulocyte-macrophage colony-stimulating factor (BMDCs) (20 ng ml^{-1}; Sigma-Aldrich) or macrophage colony-stimulating factor (BMMØ) (50 ng ml^{-1}; Sigma-Aldrich), respectively[21], and used these cells at 6 d after *in vitro* cultivation. For some of the experiments, we treated d 6 BMDCs with 0.01–1 μg ml^{-1} LPS (Sigma-Aldrich) for further activation.

Quantitation of mRNA expression. We isolated total RNA from the BMDCs by using an RNeasy kit (Qiagen), and obtained complementary deoxyribonucleic acid (cDNA) by using reverse transcriptase (RT; GE Healthcare). For quantitative analysis of RGMa mRNA expression (**Fig. 1a**), we used the cDNA as the template in a TaqMan real-time PCR assay (ABI Prism 7500 Sequence Detection System; Applied Biosystems), according to the manufacturer's protocol, and purchased specific primers and probes for the assay from Applied Biosystems. Further, we isolated total RNA from human PBMCs using Trizol (Invitrogen) and reverse-transcribed it by using a High-Capacity cDNA Reverse Transcription kit (Applied Biosystems). We examined the mRNA expression by real-time RT-PCR using

the TaqMan real-time PCR assay. We also employed TaqMan assays (Applied Biosystems) and a TaqMan Gene Expression Master Mix (Applied Biosystems) to quantify the gene expressions of IL-2 (Hs00914135_m1), IL-17a (Hs99999082_m1), IFN-γ (Hs99999041_m1), IL-4 (Hs00174122_m1), IL-10 (Hs00174086_m1), and TGF-β (Hs00998133_m1).

Next, we used SYBR Green assays to quantify mRNA expression for neogenin. We designed primers for neogenin by using Primer Express version 3.0 (Applied Biosystems), and determined the specificity of each primer set with a pretest showing the specific amplification for a specific gene by gel visualization and sequencing. We used a sample volume of 25 μl for the SYBR Green assays, which contained a 1× final concentration of Power SYBR Green PCR Master Mix (Applied Biosystems), 400 nM gene-specific primers, and 1 μl template. The PCR cycles started with an uracil-*N*-glycosylase digestion at 50°C for 2 min and an initial denaturation at 95°C for 10 min, followed by 40 cycles at 95 °C for 15 s, an annealing at 60°C for 1 min, and a gradual increase in temperature from 60 °C to 95 °C during dissociation stage. We normalized the relative mRNA expressions by measuring the amount of mRNA encoding glyceraldehyde 3-phosphate dehydrogenase in each sample, and calculated the cycle threshold values (Ct values) by using the ΔΔCt method to obtain the fold differences.

Western blotting. We lysed cells by using 2× sample buffer (250 mM Tris-HCl, 4% sodium dodecyl sulfate, 20% glycerol, 0.02% bromophenol blue, and 10% β-mercaptoethanol). After boiling for 5 min, we subjected equal volumes of the samples to 15% sodium dodecyl sulfate-polyacrylamide gel electrophoresis under reducing conditions and transferred the proteins to a polyvinylidene difluoride membrane (Immobilon-P; Millipore). After blocking it with phosphate-buffered saline (PBS) containing 5% skim milk and 0.05% Tween-20, we treated the membrane with RGMa-specific antibody[10]. For the detection, we used a horseradish peroxidase-conjugated secondary antibody (Cell Signaling Technology) and an

ECL chemiluminescence system (GE Healthcare). We quantified the protein expressions by using Scion Image software.

RGM-binding assay. We incubated splenocytes with different concentrations of human RGM-Fc for 30 min, washed and immunostained them with CD11b-specific PE-conjugated or CD4-specific APC-conjugated (BD Bioscience) antibody in combination with human Fc-specific FITC-conjugated antibodies (Sigma-Aldrich), and performed flow cytometric analysis. For analytical flow cytometry, we collected at least 10,000 events of lymphocytes on a BD Biosciences fluorescent-activated cell sorter (Calibur) and analyzed the data by using CellQuest software (BD Biosciences). We included the antibody isotype control for RGM-Fc staining and subtracted the level of background staining from the level of RGM-Fc staining.

Rap1 activity assay *in vitro* and *in vivo*. We measured Rap1 activity by using a Rap1 activation assay kit (Upstate Biotechnology). In brief, we treated $CD4^+$ T cells or splenocytes with or without 2 μg ml^{-1} of mouse recombinant RGMa (R&D Systems) for 5 min and lysed them in Mg^{2+} lysis buffer containing 25 mM *N*-2-hydroxyethylpiperazine-*N*′-2-ethanesulphonic acid (pH 7.5), 150 mM NaCl, 1% Igepal CA-630, 10 mM $MgCl_2$, 1 mM ethylenediaminetetraacetic acid, 2% glycerol, 2 mM sodium orthovanadate, 1 mM ethylsulfonyl fluoride, and protease inhibitor cocktails (Roche Diagnostics). We used cell lysates for estimating the total amount of Rap1. To precipitate active Rap1, we treated the cell lysates with the Ral-binding domain of the RalGDS–agarose conjugate for 30 min at 4 °C. We then washed the beads with the Mg^{2+} lysis buffer and resuspended them in 2× sample buffer for Western blotting using Rap1-specific antibodies (BD Bioscience) as described above.

We performed *in situ* detection of active Rap1 as described previously[22]. We fixed tissues in 4% paraformaldehyde (PFA) in 0.1 M phosphate buffer, incubated cryostat sections (10 μm) with blocking solution containing 5% bovine serum albumin (BSA) and 0.1% Triton X-100 in PBS for 1 h, and incubated them overnight at 4 °C in control glutathione S-transferase (GST) or GST-RalGDS (10 μg ml^{-1}). We washed the sections thrice, fixed them in 2% PFA in 0.1 M phosphate buffer for 10 min at room temperature, and washed them again. Then, we incubated them in GST-specific antibody (Santa Cruz Biotechnology) and CD4-specific antibody (BD Pharmingen) for 2 h at room temperature. We detected the signal by incubation with Alexa Fluor 488-conjugated antibody to mouse IgG and Alexa Fluor 546-conjugated antibody to rabbit IgG (Invitrogen) for 1 h at room temperature.

Lymphocyte-binding assay. We assessed cell adhesion as previously described[23,24]. In brief, flat-bottom Maxisorp 96-well plates (Nunc) were left uncoated (control) or precoated with 2 μg ml^{-1} recombinant mouse ICAM-1-Fc (for $CD4^+$ T cells; R&D Systems) overnight at 4 °C. We washed the plates with PBS and blocked the nonspecific binding sites with 2% BSA in RPMI-1640 medium (Invitrogen) for 1 h at 37 °C. We labeled purified $CD4^+$ T cells with 2.5 μM 2′,7′-bis-(2-carboxyethyl)-5-(and-6)-carboxyfluorescein acetoxymethyl ester (BCECF-AM; Calbiochem) for 30 min at 37 °C, followed by further washes with RPMI-1640 medium containing 0.5% BSA. We added a total of 5×10^5 cells to the precoated plates and incubated them for 1 h at 37 °C in 0.5% BSA–RPMI-1640 with or without 2 μg ml^{-1} recombinant RGMa. Where indicated, we pretreated $CD4^+$ cells with 20 μM of GGTI-298 (Calbiochem) for 1 h. We removed the nonadherent cells by washing the culture thrice with warm 0.5% BSA–RPMI-1640. We quantified adhesion by using SpectraMAX (Molecular Devices) at an excitation wavelength of 485 nm and emission wavelength of 538 nm. We quantified specific adhesion by subtracting the total number of fluorescent-positive cells in

the untreated wells. The adhesion was expressed as a ratio of specific cell attachment divided by the total input cell number.

In another experiment (**Fig. 4d**), we immunized mice with myelin oligodendrocyte glycoprotein (MOG) and complete Freund's adjuvant. At d 21 after the induction of EAE, we labeled freshly isolated $CD4^+$ T cells with BCECF-AM and incubated the cells with or without RGMa-specific antibody. We then calculated the ratio of specific cell attachment.

Immunohistochemical staining of mouse tissues. After 1, 2, and 3 weeks from EAE induction, we perfused mice transcardially with 4% PFA in PBS. We postfixed their spleen, lymph node, spinal cord, and brain tissues in the same fixatives at 4 °C overnight; soaked them in 30% sucrose and PBS; and then embedded them in optimal cutting temperature compound. We cut frozen cross-sections at 5 or 10 μm with a cryostat and mounted them on Matsunami adhesive silane-coated slides. We permeabilized the sections in PBS containing 0.1% Triton-X100, 10% goat serum, and 1% BSA for 1 h at room temperature and then incubated them with primary antibodies overnight at 4°C, followed by incubation with fluorescence-conjugated secondary antibodies for 1 h at room temperature. We used the following primary antibodies: RGMa-specific rabbit (IBL), neogenin-specific rabbit (Santa Cruz Biotech), CD11b-specific rat (Serotec), CD4-specific rat (BD Bioscience), mPDCA-1-specific rat (Miltenyi Biotec), CD11c-specific hamster (BD Bioscience), B220-specific rat (BD Bioscience), APP-specific rabbit (Invitrogen), and F4/80-specific rat (Serotec) antibodies. We used Alexa Fluor 488- or 568-conjugated goat antibody to rabbit IgG, goat antibody to rat IgG, and goat antibody to hamster IgG (Invitrogen) as the secondary antibodies. For quantification of the immunofluorescence intensities in each cell, we traced the contour of the cell manually on a counterstained image of the corresponding cell-type marker. We determined the fluorescence intensities for RGMa or neogenin within the contour

of the cell. We determined the background fluorescence of the cells by performing an identical analysis with cells labeled in the absence of the primary antibodies. We then averaged the values of the background fluorescence intensity from twenty cells and subtracted these values from the signals obtained by the immunofluorescent staining[25]. We determined the average intensities for 50–100 cells from each animal and normalized the relative intensities by using those of the controls.

To assess demyelination in the spinal cord, we performed myelin staining by using a green fluorescent lipophilic dye (FluoroMyelin, Invitrogen) according to the manufacturer's instructions; we also double-labeled the section with 4′,6-diamidino-2-phenylindole (DAPI). We identified demyelinating lesions in the ventral white matter as regions without FluoroMyelin staining.

Immunohistochemical staining of human tissues and PBMCs. We obtained tissue samples and PBMCs of individuals with MS from Chiba University, Kitasato University, and Aichi Medical University. We fixed the brain and spinal cord samples in formalin, embedded them in paraffin, and cut them in 4-μm-thick sections for immunohistochemistry. We then deparaffinized, washed, and subjected the sections to an antigen-retrieval procedure. We incubated tissue samples with human CD83-specific mouse (Serotec) or human CD209-specific (BD Pharmingen) antibodies together with human RGMa-specific antibodies (R&D System). In another experiment, we incubated the tissue samples with human CD3-specific antibody (Dako) and human neogenin-specific antibody (Santa Cruz Biotechnology). We used Alexa Fluor 488- or 568-conjugated goat anti-mouse IgG and goat anti-rat IgG (Invitrogen) as the secondary antibodies.

We sedimented the PBMCs on polyethylenimine-coated glass slides. For staining, we fixed the cells in 4% PFA in PBS and incubated them with human CD3-specific antibody and

human neogenin-specific antibody. Alexa Fluor 488-conjugated goat anti-rabbit IgG and 568-conjugated goat anti-mouse IgG (Invitrogen) were used as the secondary antibodies. We determined the fluorescence intensities for neogenin within the contour of each cell, and determined and subtracted the background fluorescence intensity. We determined the average intensities in 50–100 cells from each sample and normalized the relative intensities by using those of the controls.

EAE scoring. We assessed clinical signs of EAE on the basis of the following scale: 0, no abnormalities noted; 0.5, loss of tail tonicity; 1, loss of tail reflex; 2, loss of tail reflex, impaired righting, and paresis of one limb; 3, paresis and paralysis of one limb; 3.5, full hind limb paralysis; 4, front and hind limb paralysis; and 5, moribund or dead. We assigned intermediate scores if the neurological signs were intermediate between two scores. We obtained the mean cumulative score by averaging the total clinical scores of each mouse with EAE after immunization.

Histopathology. In the histological evaluation, we stained PFA-fixed, paraffin-embedded sections of the spinal cord with hematoxylin and eosin to assess inflammation. We examined 20–30 transverse sections from the cervical to thoracic spinal cord per mouse. We scored inflammation (inflammatory index) as follows: 0, no inflammation; 1, cellular infiltration only in the perivascular areas and meninges; 2, mild cellular infiltration in the parenchyma; 3, moderate cellular infiltration in the parenchyma; and 4, severe cellular infiltration in parenchyma[26,27].

Knockdown experiments with siRNA. We synthesized mouse RGMa siRNA (stealth siRNA,

Invitrogen) and mouse neogenin siRNA (Sigma-Genosys). The sense and antisense strands of RGMa siRNA were 5′-AAAGAGGCCGCAGUGAGUGUAGUUG-3′ and 5′-CAACUACACUCACUGCGGCCUCUUU-3′, respectively, and those of neogenin siRNA were 5′-CAAUUCCAUGGAUAGCAAU-3′ and 5′-AUUGCUAUCCAUGGAAUUG-3′, respectively. We transfected RGM siRNA, neogenin siRNA, and nontargeting double-stranded RNA (control mismatch siRNA; Invitrogen) into BMDCs and BMMØs by using Nucleofector (Amaxa, Inc.) according to the manufacturer's instructions. We estimated the transfection efficiency by using BLOCK-iT Alexa Fluor Red Fluorescent Oligo (Invitrogen) at ~50%. We collected the BMDCs and BMMØs on d 7 and washed them twice in PBS. Subsequently, we suspended 1×10^6 cells in 100 μl of nucleofection solution for mouse dendritic cells or macrophages (Amaxa, Inc.) containing 500 pmol of mouse RGMa siRNA, neogenin siRNA, or control siRNA. We transferred the samples into the certified cuvettes and placed them in the Nucleofector device. We accomplished nucleofection of the cells by using the AN-001 program (BMDCs) and Y-001 program (BMMØs). After the transfection, we cultured the cells in complete medium containing RPMI-1640 medium supplemented with glutamine, sodium pyruvate, penicillin, streptomycin, 2-ME, and 10% heat-inactivated fetal bovine serum (FBS).

GFP-labeled cell transfer and trafficking analysis. We performed cell transfer experiments by intravenous injection of 5×10^6 $CD4^+$ T cells derived from MOG-induced EAE C57BL/6-Tg (CAG-EGFP) mice into recipient wild-type mice. We immunized CAG-EGFP mice with MOG, and isolated splenocytes from them on d 7 after immunization, followed by re-stimulation with MOG for 3 d. We treated recipient mice with control or RGMa-specific antibody 3 d before and at the transfer of the restimulated $CD4^+$ T cells. Ten d after adoptive transfer, we transcardially perfused the mice with 4% paraformaldehyde in PBS. We dissected

the brain and cervical spinal cord, fixed them in the same fixatives overnight at 4 °C, and immersed them in 30% sucrose in PBS. Serial sections (20-μm thick) were cut using a cryostat and mounted on MAS-coated slides. We immunostained these sections with a rabbit GFP-specific antibody (Invitrogen) to detect EGFP-labeled cells. We counted the number of the GFP^+ T cells in sections by a standardized protocol for estimating cell density, which involved counting the number of GFP^+ T cells in the forebrain including the lateral ventricle, and the cervical spinal cord. Sections (5–10) with an individual distance of 200 μm were examined in the brain and spinal cord of the normal mice (n = 5) and RGMa-specific antibody-treated mice (n = 5).

Migration assay. We used murine brain-derived capillary endothelial cell line b-End3 (American Type Culture Collection) for this experiment. The culture medium consisted of Dulbecco's modified Eagle's medium supplemented with 2% penicillin plus streptomycin and 10% FBS. The cells were grown to confluence in the upper chamber of a 3-μm-pore 24-well transwell insert (Millipore), shown to induce and maintain blood–brain barrier characteristics *in vitro*. We evaluated barrier function in the cell monolayer by transepithelial electrical resistance measurements performed with Millicell-ERS. The resistance of blank filters as the background resistance was subtracted from the total resistance of each culture insert. At d 11 after EAE induction, we prepared $CD4^+$ T cells from MOG-EAE mice treated with control IgG or RGMa-specific antibody on d 7 and 10 after MOG immunization. We loaded a suspension of 1×10^6 $CD4^+$ T cells ml^{-1} in the upper chamber, in the presence of 10 μg ml^{-1} of RGMa-specific antibody or control antibody. We assessed the ability of $CD4^+$ T cells to cross the monolayer by counting the number of cells that transmigrated to the lower chamber after 18 h.

Adoptive transfer experiments. For the adoptive transfer of macrophages with neogenin knockdown, we injected CD11b-DTR mice intravenously with 5×10^6 live BMMØs with or without neogenin knockdown. Because CD11b is positive for certain dendritic cells, we injected mice simultaneously with 5×10^6 BMDCs. We then immunized the mice with MOG, injected subcutaneously with 0.2 ml CFA containing 500 μg of *Mycobacterium tuberculosis*. Recipient mice received 200 ng of pertussis toxin intravenously 48 h after the MOG immunization. For ablation of resident macrophages, we injected the CD11b-DTR mice intraperitoneally with 25 ng g^{-1} diphtheria toxin (Sigma) on d –1 and 3 after the MOG immunization.

Intrathecal administration of RGMa-specific antibody in EAE mice. On d 7 after the MOG-EAE induction, we fitted the mice with an osmotic minipump (100 μl solution, 0.5 μl h^{-1}, 7-d delivery; Alzet pump model 1007D) filled with control rabbit IgG (22.3 μg kg^{-1} d^{-1} over 1 week; Sigma-Aldrich) or RGMa-specific antibody (22.3 μg kg^{-1} d^{-1} over 1 week). This antibody dose has been shown to be effective in inhibiting the effect of RGMa in the CNS[10]. We placed the minipump under the skin of the animal's back and connected a Silastic tube to the minipump under the dura of the thoracic cord. We sutured the tube just caudal to the laminectomy site to anchor it in place. Afterward, we sutured the muscle and skin layers.

Animal model of spinal cord injury and behavioral analysis. We anesthetized female C57BL/6 mice with sodium pentobarbital (40 mg kg^{-1}) and performed laminectomy at the T9–T10 vertebral level. The mice then received a moderate (60 kdyn) contusion injury with an Infinite Horizons impactor. We intraperitoneally administered 400 μg of RGMa-specific or control antibody (rabbit IgG; Sigma-Aldrich) to the mice on d 0 and 3 after the injury. To assess their functional recovery after the injury, two blinded observers tested the mice by

using the open-field Basso Mouse Scale (BMS)[28] on d 1, 3, and 5, and once a week thereafter until the end of the study. We plotted the mean scores per treatment group as a function of the time post-injury. We also performed manual bladder expression twice a day until reflex bladder emptying was established. We had assessed the animals before the injury to ensure the absence of deficits in hind limb function and expose them to an open-field testing environment.

PBMC isolation and stimulation. We isolated all PBMCs freshly by using standard Ficoll-Hypaque centrifugation within 24 h of venipuncture and immediately applied them to the following assays. We pretreated PBMCs with 10 μg ml^{-1} of mouse monoclonal human RGMa-specific antibody, which we generated, or with control IgG for 30 min and then stimulated them with PMA (10 ng ml^{-1}) and ionomycin (1 μg ml^{-1}) (both from Sigma-Aldrich) in RPMI-1640 medium supplemented with glutamine, sodium pyruvate, penicillin, streptomycin, 2-ME, and 10% heat-inactivated FBS. We estimated the cell proliferation by measuring the BrdU incorporation and estimated the production of *IL-2*, *IFN-γ*, *IL-17*, *IL-4*, *IL-10*, and *TGF-β* by RT-PCR analysis.

Biodistribution of RGMa-specific antibody. We administered RGMa-specific antibody (400 μg intraperitoneally) to mice on d 0 and 2. We anesthetized the mice and removed their spleen, lymph node, spinal cord, and brain tissues on d 7 for biodistribution analysis of RGMa-specific antibody. We lysed the tissues and subjected them to Western blotting with horseradish peroxidase-conjugated rabbit IgG antibody (Cell Signaling Technology). We also administered RGMa-specific antibody by intraperitoneal injection to the mice on d 7 and 10 after the MOG immunization and assessed the biodistribution on d 11.

Intracellular staining. We analyzed intracellular cytokine expressions in freshly isolated splenocytes stimulated with CD3-specific antibody in the presence of 10 μg ml^{-1} Brefeldin A (Sigma-Aldrich) for 6 h. After staining the cells with a phycoerythrin-conjugated CD4-specific antibody (BD Biosciences), we fixed and permeabilized (Cytofix/Cytoperm and Perm/Wash buffer; BD Biosciences) and stained them with FITC-conjugated IL-4- or IL-10-specific (BD Biosciences) antibody, and then analyzed the results fluorocytometrically (FACSCalibur; BD Biosciences).

SUPPLEMENTARY REFERENCES

21. Lutz, M.B. *et al.* An advanced culture method for generating large quantities of highly pure dendritic cells from mouse bone marrow. *J. Immunol. Methods* **223**, 77–92 (1999).

22. Taniguchi, J. *et al.* Rap1 is involved in the signal transduction of myelin-associated glycoprotein. *Cell Death Differ.* **15**, 408–419 (2008).

23. Sebzda, E., Bracke, M., Tugal, T., Hogg, N. & Cantrell, D.A. Rap1A positively regulates T cells via integrin activation rather than inhibiting lymphocyte signaling. *Nat. Immunol.* **3**, 251–258 (2002).

24. Duchniewicz, M. *et al.* Rap1A-deficient T and B cells show impaired integrin-mediated cell adhesion. *Mol. Cell Biol.* **26**, 643–653 (2006).

25. Alexander, J.K. *et al.* Ric-3 promotes α7 nicotinic receptor assembly and trafficking through the ER subcompartment of dendrites. *J. Neurosci.* **30**, 10112–10126 (2010).

26. Okuda, Y., Okuda, M. & Bernard, C.C. The suppression of T cell apoptosis influences the severity of disease during the chronic phase but not the recovery from the acute phase of experimental autoimmune encephalomyelitis in mice. *J. Neuroimmunol.* **131**, 115–125 (2002).

27. Liu, J. *et al.* TNF is a potent anti-inflammatory cytokine in autoimmune-mediated demyelination. *Nat. Med.* **4**, 78–83 (1998).

28. Basso, D.M. *et al.* Basso Mouse Scale for locomotion detects differences in recovery after spinal cord injury in five common mouse strains. *J. Neurotrauma* **23**, 635–659 (2006).

The EMBO Journal (2011) 30, 1389–1401 | © 2011 European Molecular Biology Organization | All Rights Reserved 0261-4189/11
www.embojournal.org

THE EMBO JOURNAL

Myelin suppresses axon regeneration by PIR-B/SHP-mediated inhibition of Trk activity

Yuki Fujita[1,2], Shota Endo[3], Toshiyuki Takai[3] and Toshihide Yamashita[1,2,*]

[1]Department of Molecular Neuroscience, Graduate School of Medicine, Osaka University, Osaka, Japan, [2]JST, CREST, Tokyo, Japan and [3]Department of Experimental Immunology and CREST Program of JST, Institute of Development, Aging and Cancer, Tohoku University, Sendai, Japan

Paired immunoglobulin-like receptor B (PIR-B) partially mediates the regeneration-inhibiting effects of the myelin-derived protein Nogo, myelin-associated glycoprotein (MAG), and oligodendrocyte-myelin glycoprotein (OMgp). In this study, we report that inhibition of the PIR-B signaling cascades in neurons enhances axon regeneration in the central nervous system (CNS). Binding of MAG to PIR-B led to the association of PIR-B with tropomyosin receptor kinase (Trk) neurotrophin receptors. Src homology 2-containing protein tyrosine phosphatase (SHP)-1 and SHP-2, which were recruited to PIR-B upon MAG binding, functioned as Trk tyrosine phosphatases. Further, SHP-1 and SHP-2 inhibition reduced MAG-induced dephosphorylation of Trk receptors and abolished the inhibitory effect of MAG on neurite growth. Thus, PIR-B associated with Trk to downregulate basal and neurotrophin-regulated Trk activity through SHP-1/2 in neurons. Moreover, *in vivo* transfection of small interfering RNA (siRNA) for SHP-1 or SHP-2 induced axonal regeneration after optic nerve injury in mice. Our results thus identify a new molecular target to enhance regeneration of the injured CNS.

The EMBO Journal (2011) **30,** 1389–1401. doi:10.1038/emboj.2011.55; Published online 1 March 2011
Subject Categories: neuroscience
Keywords: axon regeneration; myelin; paired immunoglobulin-like receptor B (PIR-B); Src homology 2-containing protein tyrosine phosphatase (SHP); tropomyosin receptor kinase (Trk)

Introduction

Myelin-derived inhibitors of axonal regeneration have an important role in inhibiting regeneration in the adult central nervous system (CNS) (Yiu and He, 2006). Three myelin-derived proteins possess potent inhibitory activity for neurite growth *in vitro* by interacting with the Nogo receptor (NgR). However, in a previous *in vitro* study, researchers have reported that genetic deletion of NgR does not reduce neurite growth inhibition by myelin-derived proteins (Zheng *et al*, 2005). This observation suggested the existence of other hitherto unidentified binding receptors for these inhibitors. Later, paired immunoglobulin-like receptor B (PIR-B)—a major histocompatibility complex (MHC) class I receptor (Takai, 2005)—was identified as a second receptor (Atwal *et al*, 2008). PIR-B is expressed on various haematopoietic cells as well as on neurons (Syken *et al*, 2006). It binds not only to the 66-amino acid long Nogo-66, which is one of the two inhibitory domains of Nogo, but also to myelin-associated glycoprotein (MAG) and oligodendrocyte-myelin glycoprotein (OMgp). Further, the presence of PIR-B is essential for inhibition of neurite growth mediated by Nogo-66 and other myelin proteins (Atwal *et al*, 2008). It is unknown whether PIR-B inhibition promotes axonal regeneration after injury to the CNS *in vivo*. Nonetheless, the role of PIR-B in restricting plasticity during development is supported by the fact that deprivation-induced expansion of the open eye's territory is more robust and can be properly induced after the critical developmental period in mice expressing PIR-B lacking the transmembrane domain (PIR-B-TM mice) (Syken *et al*, 2006). Therefore, we considered that elucidating the molecular mechanism underlying PIR-B signaling in neurons should increase our knowledge on the inability of injured axons to regenerate as well as on the plasticity of the developing CNS.

PIR-B contains immunoreceptor tyrosine-based inhibitory motifs. Phosphorylation of these sites upon ligand binding leads to Src homology 2-containing protein tyrosine phosphatase (SHP)-1 and SHP-2 recruitment to PIR-B, which then modulates immune signal transduction pathways. PIR-B isolated from the brain is also phosphorylated and associated with SHP-1 and SHP-2 (Syken *et al*, 2006). Thus, it would be of interest to elucidate the signaling mechanism of PIR-B in neurons by determining whether SHP phosphatase recruitment occurs upon ligand stimulation and to clarify whether SHP mediates PIR-B signaling in neurons. Thus, we aimed to identify the molecular targets of SHP-1 and SHP-2. SHP-1 has been shown to interact with and dephosphorylate several growth factor receptors, including insulin-like growth factor-1 (IGF-1), platelet-derived growth factor (PDGF), and epidermal growth factor (EGF) receptors (Tonks and Neel, 2001). Interestingly, a previous study reported that SHP-1 dephosphorylates the tropomyosin receptor kinase A (TrkA) receptor, a nerve growth factor (NGF) receptor, in PC12 cells and sympathetic neurons. Further, an enhanced association of SHP-2 with the TrkB receptor—a brain-derived neurotrophic factor (BDNF) receptor—inhibits BDNF-induced TrkB autophosphorylation and activation in cerebellar neurons (Rusanescu *et al*, 2005). These findings prompted us to hypothesize that Trk receptors are PIR-B targets in neurons (Marsh *et al*, 2003).

*Corresponding author. Department of Molecular Neuroscience, Graduate School of Medicine, Osaka University, 2-2 Yamadaoka, Suita, Osaka 565-0871, Japan. Tel.: +81 66 879 3661; Fax: +81 66 879 3669; E-mail: yamashita@molneu.med.osaka-u.ac.jp

Received: 19 October 2010; accepted: 4 February 2011; published online: 1 March 2011

In the present study, we demonstrated that PIR-B binds to and inactivates Trk neurotrophin receptors, which are known to promote neurite growth in neurons. Upon MAG activation, PIR-B recruited SHP-1 and SHP-2, which in turn dephosphorylated the Trk receptors. We suggest that reduced Trk receptor activity results in MAG-induced neurite growth inhibition. Further, the inhibition of SHP promoted axonal regeneration of the injured optic nerve *in vivo*.

Results

Trk receptors are PIR-B targets

We first examined whether PIR-B interacted with Trk receptors. COS-7 cells were transfected with haemagglutinin (HA)-tagged full-length TrkB (HA–TrkB FL) and/or full-length PIR-B constructs. The cell extracts were immunoprecipitated with anti-PIR-B or anti-HA antibodies (Figure 1A and B). Of

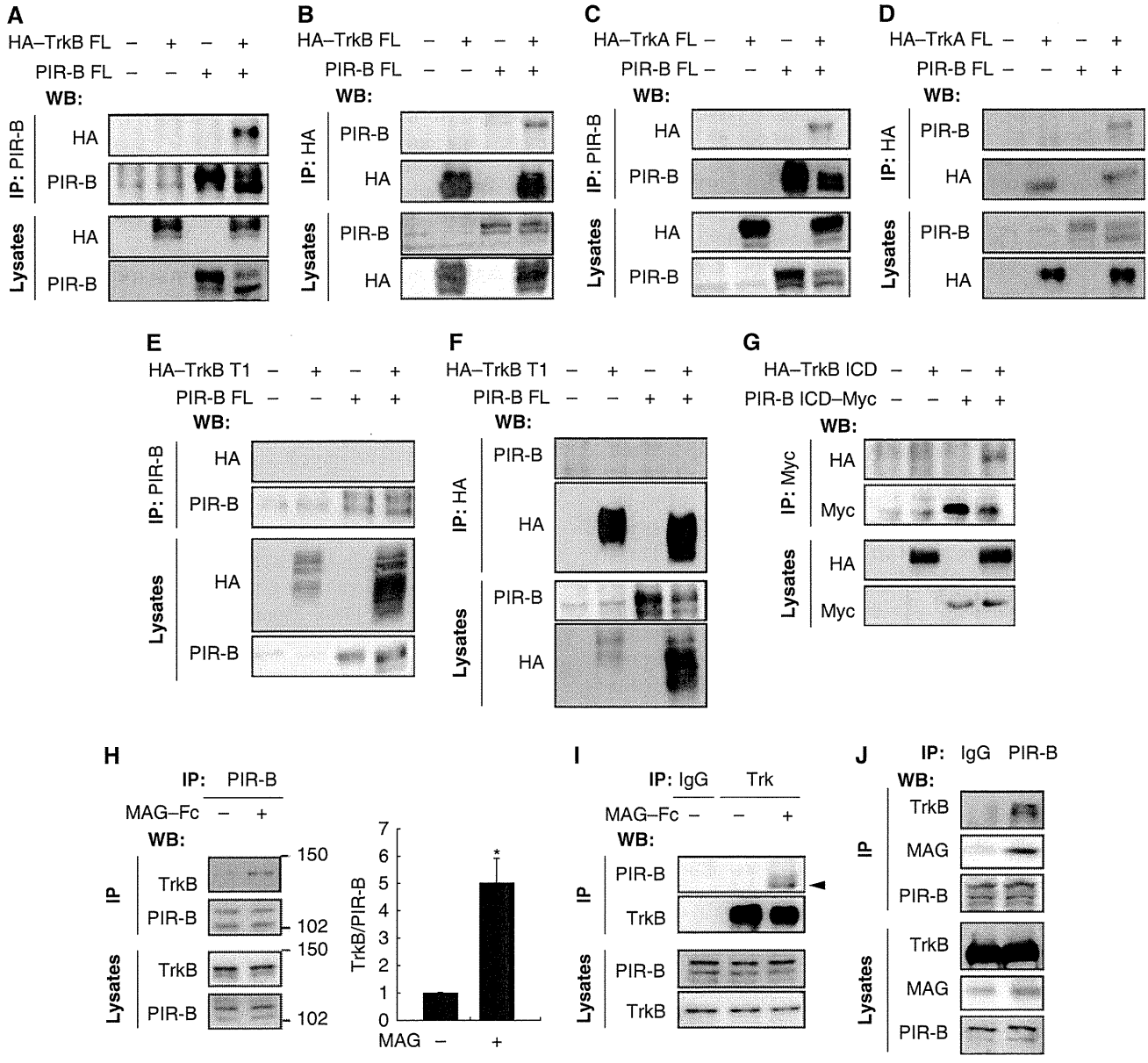

Figure 1 Ligand-dependent association of PIR-B with TrkB. (**A**, **B**) Co-immunoprecipitation of full-length PIR-B (PIR-B FL) with HA-tagged full-length TrkB (HA–TrkB FL). COS-7 cells were transiently transfected with the indicated plasmids. Cell lysates were immunoprecipitated with anti-PIR-B (**A**) or anti-HA (**B**) antibodies. The immunoprecipitates (IP) and cell lysates (lysates) were analysed by immunoblotting with anti-HA and anti-PIR-B antibodies. (**C**, **D**) Co-immunoprecipitation of PIR-B FL with HA-tagged full-length TrkA (HA–TrkA FL). COS-7 cells were transiently transfected with the indicated plasmids. Cell lysates were immunoprecipitated with anti-PIR-B (**C**) or anti-HA (**D**) antibodies. Western blotting was performed using the indicated antibodies. (**E**, **F**) PIR-B and HA-tagged TrkB T1 did not interact in the transfected COS-7 cells. Co-immunoprecipitation was carried out as shown in (**A**, **B**). (**G**) Co-immunoprecipitation of Myc-tagged PIR-B ICD (PIR-B ICD–Myc) with HA-tagged TrkB ICD (HA–TrkB ICD) using anti-Myc antibodies. (**H**, **I**) Association of endogenous PIR-B with TrkB in CGNs. CGNs were left untreated or were treated with MAG–Fc (25 μg/ml) for 15 min. Lysates prepared from the CGNs were immunoprecipitated with anti-PIR-B (**H**) or anti-pan Trk (**I**) antibodies, followed by immunoblotting with anti-TrkB and anti-PIR-B antibodies, respectively. The association between PIR-B and TrkB was observed in MAG-treated cells. IgG, control IgG. The arrowhead indicates the band corresponding to PIR-B. The TrkB signal intensity was quantified by densitometry and normalized to the signal intensity of precipitated PIR-B (**H**). $^*P<0.05$ by Welch's *t*-test. (**J**) Interaction of PIR-B with TrkB and MAG in the mouse brain. Lysates prepared from whole mouse brain were immunoprecipitated with anti-PIR-B antibodies, followed by western blotting for TrkB and MAG.